

Line Waves in Non-Hermitian Metasurfaces

Massimo Moccia, Giuseppe Castaldi, Andrea Alù, and Vincenzo Galdi*



Cite This: <https://dx.doi.org/10.1021/acsphtronics.0c00465>



Read Online

ACCESS |

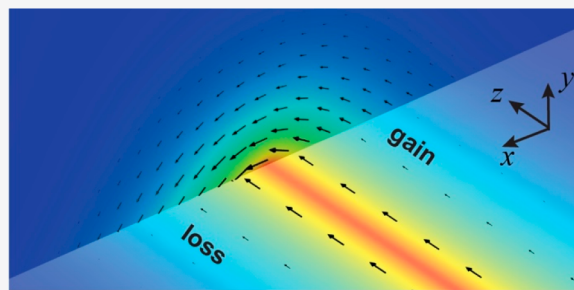
Metrics & More

Article Recommendations

Supporting Information

ABSTRACT: Planar junctions between reactive surface impedances with dual character (capacitive/inductive) can sustain line waves localized both in-plane and out-of-plane around the discontinuity, which propagate unattenuated along one-dimensional paths. Due to their attractive properties, these waves are of potential interest in applications ranging from integrated photonics to optical sensing. Here, we introduce and explore a non-Hermitian platform supporting these exotic modes based on parity-time symmetry. Specifically, we show that line waves can occur in the presence of a uniform surface reactance (either capacitive or inductive) and a symmetric resistance discontinuity from negative to positive values (i.e., gain and loss). We study analytically and numerically the propagation properties of these waves and the underlying physical mechanisms and also illustrate their intriguing properties in terms of confinement, reconfigurability, spin-momentum locking and lasing. Finally, we address possible practical implementations based on photoexcited graphene. Our results hold intriguing potentials for applications in flat optics and reconfigurable photonics.

KEYWORDS: metasurfaces, line-waves, non-Hermitian, lasing, graphene



Metasurfaces are artificially textured surfaces, with an electrical thickness much smaller than the wavelength, engineered to manipulate the amplitude, phase, and polarization of electromagnetic wavefronts. Although the basic concept of spatially modulating the surface impedance is of longstanding interest in electrical engineering,¹ the interest in this topic has witnessed an exponential increase in the past decade, sparked by the seminal work by Yu et al.² on generalized Snell's laws of reflection and refraction.

Besides enabling unprecedented capabilities in the control of reflection and transmission properties, the newly established field of flat optics has also provided new perspectives in the manipulation of surface waves.^{3,4} In conjunction with the disruptive emergence of two-dimensional (2-D) materials,⁵ this progress has, in turn, inspired the planar transposition of several intriguing concepts borrowed from volumetric metamaterials, including, for example, hyperbolic propagation⁶ and transformation optics.^{7–11}

More recently, theoretical¹² and experimental¹³ studies have demonstrated the existence of a new type of surface wave that can propagate along an abrupt discontinuity between metasurfaces characterized by dual (capacitive/inductive) surface reactances. These waves maintain the out-of-plane localization that is typical of conventional surface waves on reactive metasurfaces, but they also exhibit in-plane localization along the discontinuity, thereby transporting the energy along a 1-D track. Accordingly, in what follows, we will refer to them as "line waves", although other terms, such as "one-dimensional waves" or "edge modes", have also been utilized, in

connection with the mounting interest in topological edge modes.¹⁴

Line waves exhibit intriguing properties in terms of field enhancement, bandwidth, propagation-dependent polarization, robustness, and potential reconfigurability, which appear promising for a variety of applications, ranging from integrated photonics to optical sensing. More recently, graphene-based implementations have been suggested for the active manipulation of terahertz waves,¹⁵ and topological concepts related to these phenomena have been explored.¹⁶

Against this background, we introduce here a new form of line waves that can be sustained at a planar surface-impedance discontinuity characterized by the same reactance but opposite signed resistance (i.e., gain and loss). Unlike conventional line waves, the underlying localization mechanism does not rely on the duality principle, but rather on parity-time (PT) symmetry. Such a concept, originally proposed by Bender and co-workers,¹⁷ as the foundation of a non-Hermitian extension of quantum mechanics, has broadly resonated in many fields of physics,¹⁸ and especially in optics and photonics.^{19,20} In particular, non-Hermitian metasurfaces characterized by spatial modulation of gain and loss have been recently proposed for applications including negative refraction and focusing.²¹

Received: March 24, 2020

Published: June 30, 2020

unidirectional cloaking,²² imaging,^{23,24} sensing,^{25,26} lasering,^{21,23–28} and absorbers.²⁸ Interestingly, in all these scenarios, the gain/loss constituents are stacked out-of-plane, along the propagation direction. To the best of our knowledge, our study here is the first to address phenomena associated with in-plane gain-loss modulations, across the propagation direction.

In the following, we study the propagation of line waves in non-Hermitian metasurfaces both analytically (by applying the Sommerfeld–Maliuzhinets approach developed for conventional line waves²⁹) and numerically (via finite-element simulations) and explore possible applications and technologically feasible implementations.

RESULTS AND DISCUSSION

Geometry and Formulation. Referring to the schematic in Figure 1, we consider a planar metasurface laying in vacuum

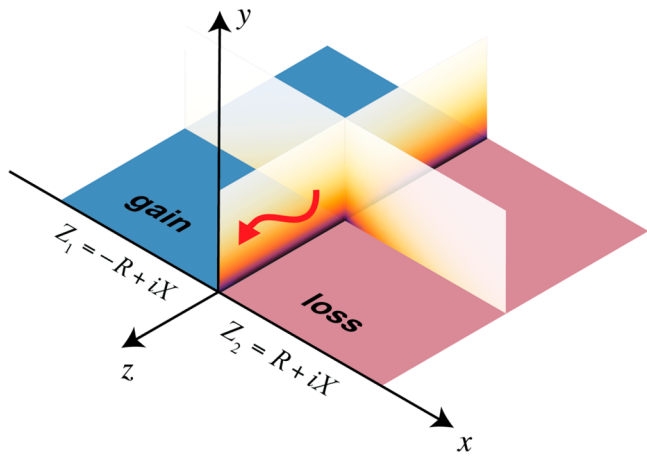


Figure 1. Problem geometry. PT-symmetric metasurface junction in the x - z plane supporting a non-Hermitian line wave. The false-color maps qualitatively illustrate the unattenuated propagation along the z -direction and the in-plane and out-of-plane decay around the interface $x = 0$.

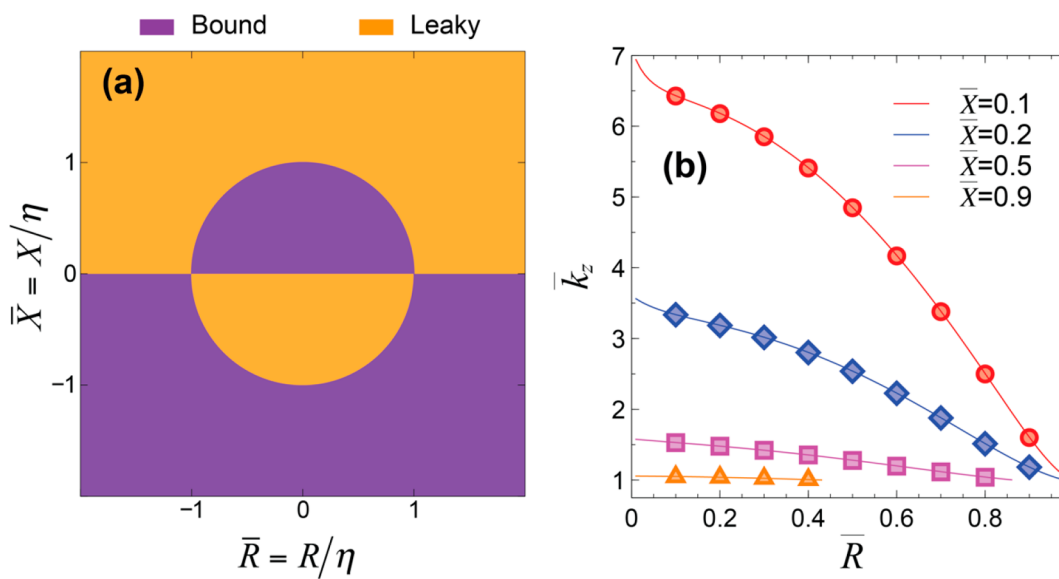


Figure 2. Eigenmode analysis. (a) Partition of the normalized-impedance complex plane identifying the parameter regions corresponding to bound (purple-shaded) and leaky (orange-shaded) modes. (b) Effective index of bound modes as a function of the gain/loss parameter, for representative values of the normalized (capacitive) reactance; solid curves and markers pertain to analytic and numerical (finite-element) solutions, respectively.

on the x - z plane of a 3-D Cartesian system, characterized by an isotropic impedance boundary condition^{30,31}

$$\mathbf{E}_t = Z(x)\mathbf{u}_y \times \mathbf{H}|_{y=0} \quad (1)$$

where subscript “ t ” denotes the tangential component, and \mathbf{u}_y is a y -directed unit vector. We assume a time-harmonic $\exp(-i\omega t)$ dependence and a piecewise continuous impedance distribution, with a discontinuity at the $x = 0$ interface:

$$Z(x) = \begin{cases} Z_1 = -R + iX, & x < 0 \\ Z_2 = R + iX, & x > 0 \end{cases} \quad (2)$$

which satisfies the PT-symmetry condition

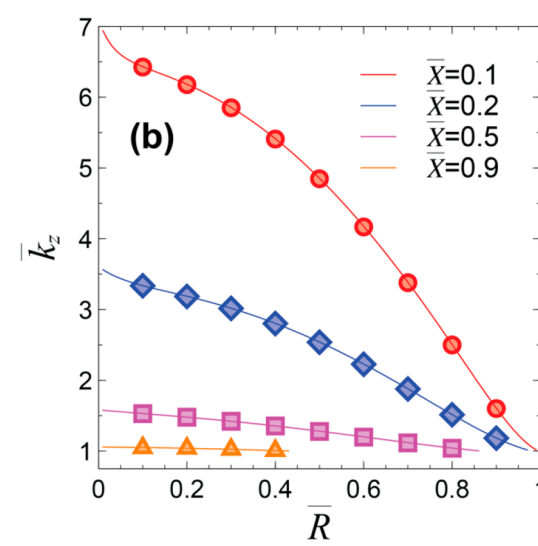
$$Z(x) = -Z^*(-x) \quad (3)$$

Without loss of generality, we consider $R > 0$, which, for the assumed time convention, implies that the regions 1 ($x < 0$) and 2 ($x > 0$) exhibit gain and loss, respectively.

In the absence of gain/loss ($R = 0$), the structure reduces to a uniform, reactive surface that, as is well known,¹³ supports surface waves with transverse-electric (TE) or transverse-magnetic (TM) polarization for inductive ($X < 0$) or capacitive ($X > 0$) reactance, respectively. These surface waves propagate unattenuated in the x - z plane with propagation constants¹³

$$k_p = \begin{cases} k\sqrt{1 + \left(\frac{\eta}{X}\right)^2}, & \text{TE} \\ k\sqrt{1 + \left(\frac{X}{\eta}\right)^2}, & \text{TM} \end{cases} \quad (4)$$

and decay exponentially along the y -direction (i.e., out of plane). In eq 4, ρ denotes an arbitrary in-plane direction, while $k = \omega\sqrt{\epsilon_0\mu_0} = 2\pi/\lambda$ and $\eta = \sqrt{\mu_0/\epsilon_0}$ are the wavenumber and intrinsic impedance of vacuum, respectively (and λ the corresponding wavelength).



As we will show hereafter, the discontinuity in the surface resistance may induce an additional in-plane localization around the $x = 0$ interface. In the specific PT-symmetric scenario of interest, due to the gain–loss balance, such line waves can propagate without attenuation along the discontinuity, with a propagation function $\exp(ik_z z)$ and a real-valued propagation constant k_z , while exhibiting both in-plane and out-of-plane localization, as schematically illustrated in Figure 1. To some extent, this propagation scenario can be interpreted as the lower-dimensional 1-D analog of the surface waves supported at the interfaces between PT-symmetric metamaterial slabs.^{32–34}

Eigenmode Analysis. For conventional line waves, an approximate analytical solution for the eigenmode (source-free) problem was proposed¹² in the electrostatic limit $k_z \gg k$. More recently, an exact analytic treatment was put forward²⁹ by suitably adapting a generalization of the Sommerfeld–Maliuzhinets method for the scattering from impedance wedges.^{35,36} Such an approach is not restricted to the case of dual reactive impedances and can, therefore, be applied to the PT-symmetric scenario of interest here. Accordingly, as detailed in the Supporting Information, we can rigorously derive the dispersion equation that relates the propagation constant³⁴ to the surface impedances $Z_{1,2}$ and frequency. We are especially interested in bound modes characterized by real-valued propagation constant $|k_z| > k$. In what follows, we focus on forward-propagating waves ($k_z > 0$) and normalize the relevant quantities with respect to their values in vacuum, introducing the effective index $\bar{k}_z = k_z/k$ and normalized impedances $\bar{Z}_{1,2} = Z_{1,2}/\eta$. As illustrated by the partition in Figure 2a (see Supporting Information for details), depending on the reactance sign, bound modes (i.e., $\bar{k}_z > 1$) occur inside or outside the unit circle in the normalized-impedance complex plane (purple-shaded regions), namely,

$$\begin{cases} |\bar{Z}| < 1, & X > 0 \\ |\bar{Z}| > 1, & X < 0 \end{cases} \quad (5)$$

where the impedance magnitude does not depend on the subscript. The complementary (orange-shaded) regions correspond to leaky modes,³⁷ which are complex in nature, lie within the light cone and couple to the radiation continuum; they are beyond the scope of this study. The unit-circle boundary $|\bar{Z}| = 1$ corresponds to the light cone, $\bar{k}_z = 1$ (see the Supporting Information for details) and, therefore, separates the bound and leaky regimes. Note that negative values of \bar{R} only imply interchanging the gain and loss regions, which does not affect the bound/leaky character of the mode.

For capacitive surfaces ($X > 0$), Figure 2b shows the effective index as a function of the gain/loss parameter $\bar{R} = R/\eta$, for representative values of the normalized reactance $\bar{X} = X/\eta$. Also shown (as markers) are the values computed numerically via finite-element simulations, showing excellent agreement (average error of 0.15%).

The corresponding modal fields can be computed by integrating in the complex plane²⁹ and, similar to conventional line waves, exhibit a singular value³⁸ at the interface $x = y = 0$, while maintaining a finite energy. Figure 3 shows a representative modal field distribution, in the plane orthogonal to the propagation direction, numerically computed via finite-element simulations. Besides the anticipated in-plane and out-of-plane localization, we observe from the inset in Figure 3a that there is a transverse power flow from the gain to the loss

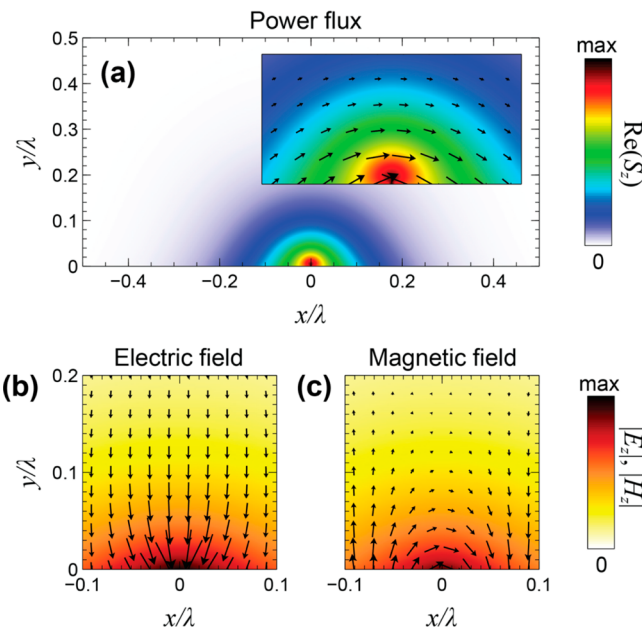


Figure 3. Eigenmode analysis. (a–c) Numerically computed powerflux (real part of Poynting vector S), electric and magnetic fields, respectively, for $\bar{R} = 0.5$ and $\bar{X} = 0.5$ (effective index $\bar{k}_z = 1.277$). The z -components are shown as false-color maps, whereas the corresponding x and y components are shown as vector plots.

region, which sustains unattenuated propagation along the z -direction. The presence of such transverse power flow, which represents an important difference compared to conventional line waves,¹³ is quite intriguing, as it cannot arise in Hermitian systems, and it can be associated with anomalous forces arising in the near-field of these line waves,³⁹ of interest for microfluidics and micro-optomechanical systems. Moreover, from Figure 3b,c, we observe that the transverse field distributions are quite different from those of conventional line waves.¹³ In particular, for the capacitive case under study, the magnetic field exhibits handedness (which flips for $k_z < 0$) that can be associated with spin-momentum locking, whereas the electric field does not. We also highlight the hybrid character of the modal fields, with generally nonzero electric and magnetic components along the propagation direction.

For the capacitive scenario in Figures 2b and 3, it can be shown (see Figure S1 of the Supporting Information) that, for a given value of \bar{R} , the localization mechanism becomes more effective for decreasing values of \bar{X} . For fixed \bar{X} , the in-plane localization varies nonmonotonically with \bar{R} , but it eventually deteriorates up to being completely lost for vanishing \bar{R} . Consistent with Figure 2b, in the limit $\bar{R} \rightarrow 0$ (uniform capacitive surface), the effective index becomes

$$\bar{k}_z = \sqrt{\frac{1 + \left(\frac{1}{\bar{X}}\right)^2}{2}} \quad (6)$$

which differs by a factor $\sqrt{2}$ from the expression in eq 4. This seeming inconsistency is explained by observing that the eigenmode solution has an x -directed component of the wave vector, responsible for confining the fields at the interface when $\bar{R} > 0$; in the limit $\bar{R} \rightarrow 0$, $|\bar{k}_x| = |\bar{k}_z|$, and hence, the actual effective index $\bar{k}_p = \sqrt{\bar{k}_x^2 + \bar{k}_z^2} = \sqrt{1 + (1/\bar{X})^2}$ is consistent with eq 4. In other words, as $\bar{R} \rightarrow 0$, the considered modes

correspond to surface waves traveling over an isotropic capacitive surface at 45° between the x and z axes.

The above observations also indicate that the effective index diverges in the limit $|\bar{Z}| \rightarrow 0$, thereby implying that an arbitrarily large localization can be, in principle, attained in the limit of a low-impedance surface. Together with the field singularity at the interface $x = y = 0$, this is an effect of the idealized impedance discontinuity assumed in our model. As shown in [Figure S2 of the Supporting Information](#), both effects are washed out if a more realistic model featuring a smooth impedance transition is considered.

Finally, we observe that the inductive case ($X < 0$) can be straightforwardly addressed by resorting to the duality principle.⁴⁰ It can be shown (see the [Supporting Information](#) for details) that the analytic dispersion equation is invariant with respect to the duality transformation

$$Z \rightarrow \frac{\eta^2}{Z} \quad (7)$$

This implies that, for an inductive configuration featuring surface admittances $Y_{1,2} = +G + iB$ (with $B > 0$), the dispersion properties can be obtained directly from [Figure 2b](#), by considering the normalized conductance $\bar{G} = \eta G$ in place of \bar{R} and the normalized susceptance $\bar{B} = \eta B$ in place of \bar{X} .

An example of a modal field for an inductive configuration, dual of the one in [Figure 3](#), is shown in [Figure S3 of the Supporting Information](#). By comparison with [Figure 3](#), we observe the same effective index and field distributions, with electric and magnetic fields interchanged.

Source-Excited Configurations. In order to ascertain the actual excitability of the above eigenmode solutions, we carry out 3-D numerical simulations in the presence of sources. With specific reference to the parameter configuration in [Figures 3](#) and [4a,b](#), the in-plane and out-of-plane field distributions for a structure excited by an elementary electric dipole are shown, which are fully consistent with the eigenmode solution. It is

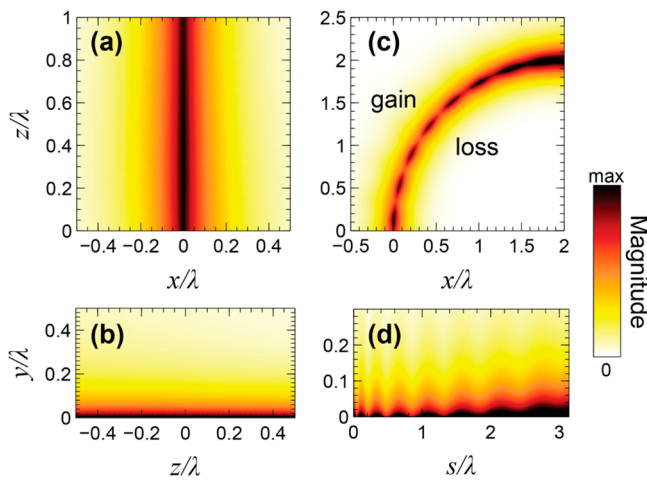


Figure 4. Source-excited straight and curved configurations. (a, b) Numerically computed in-plane ($y = 0.01\lambda$) and out-of-plane ($x = 0$) electric-field magnitude maps in false-color scale, respectively, for a straight PT-symmetric impedance junction with $\bar{R} = 0.5$ and $\bar{X} = 0.5$. (c, d) Corresponding maps for a curved section (circular arc of radius λ); the out-of-plane cut is taken along the circular gain-loss interface, with s denoting the curvilinear abscissa. The field is excited by a y -directed elementary electric dipole placed at $x = 0$, $y = 0.02\lambda$, and $z = -0.5\lambda$ (outside the domains visualized).

also insightful to look at the propagation along nonstraight paths. [Figure 4c,d](#) shows a representative example of a curved trajectory (circular arc). It can be observed that the in-plane and out-of-plane confinement is maintained even for nonstraight paths, but, due to the curvature, gain and loss are no longer perfectly balanced and therefore the propagation constant along the curvilinear abscissa becomes complex-valued. For the parameter configurations in [Figure 4c,d](#), this interestingly corresponds to amplification for clockwise propagation and attenuation for counterclockwise. Clearly, the situation is reversed when interchanging gain and loss or the curvature sign. More complex examples, featuring S-shaped and piecewise-straight paths, are shown in [Figure S4 of the Supporting Information](#).

[Figure 5](#) illustrates the effects of gain–loss (im)balance and the leakage that occurs when the condition in [eq 5](#) is not verified. Specifically, [Figure 5a,b](#) show in-plane and out-of-plane field distribution pertaining to the configuration in [Figure 4a,b](#), but in the absence of gain (i.e., $\bar{Z}_1 = i0.5$, $\bar{Z}_2 = 0.5 + i0.5$). As expected, the out-of-plane confinement is still maintained. However, propagation along the interface $x = 0$ is substantially damped in view of the prevailing lossy character. Interestingly, looking at the in-plane field distribution ([Figure 5a](#)), in the (now fully reactive) $x < 0$ half, we observe an extended character with directional properties. This suggests some potentially interesting applications for reconfigurable photonics, with the possibility to switch between an extended and a strongly localized behavior by (de)activating the gain. Moreover, this result shows that, even in fully passive configurations, a suitable spatial modulation of the surface resistance may induce interesting in-plane routing responses. [Figures 5c and 5d](#) show instead the field distributions pertaining to a gain-loss balanced configuration with $\bar{Z}_{1,2} = +1.1 + i0.1$, which does not satisfy the bound-mode condition in [eq 5](#). As anticipated, and clearly visible in [Figure 5d](#), in this case the out-of-plane confinement is lost, as the field can couple with the radiation continuum. As observed from [Figure 5c](#), the propagation along the z -axis is attenuated as the power progressively leaks out-of-plane. The (far-field) radiation pattern shown in [Figure 5e](#) is consistent with leaky-wave radiation.⁴¹

Finally, we note that our non-Hermitian line waves possess inherent spin-momentum locking properties, consistent with evanescent waves and plasmon propagation.⁴² Similar to conventional line-waves,¹³ they exhibit chiral-coupling properties with respect to circularly polarized sources. This is illustrated in [Figure 6](#), which shows that a circularly polarized elementary source placed at $x = 0$ can excite unidirectional propagation along the gain-loss interface with direction depending on its handedness. This unidirectional excitation is progressively lost if the source is displaced along the x -direction. One can therefore envision intriguing applications to chiral quantum optics and valleytronics.⁴³

Imbalanced Configurations and Lasing Conditions.

One of the intriguing features of non-Hermitian line waves, also in comparison with Hermitian ones, is their potential applicability to flat-optics lasing and coherent-perfect-absorption scenarios. [Figure 7a](#) schematizes a possible configuration where a PT-symmetric impedance junction is perturbed by introducing an imbalanced section

$$\bar{Z}_1 = -(\bar{R} + \delta) + i\bar{X}, \bar{Z}_2 = \bar{R} + i\bar{X} \quad (8)$$

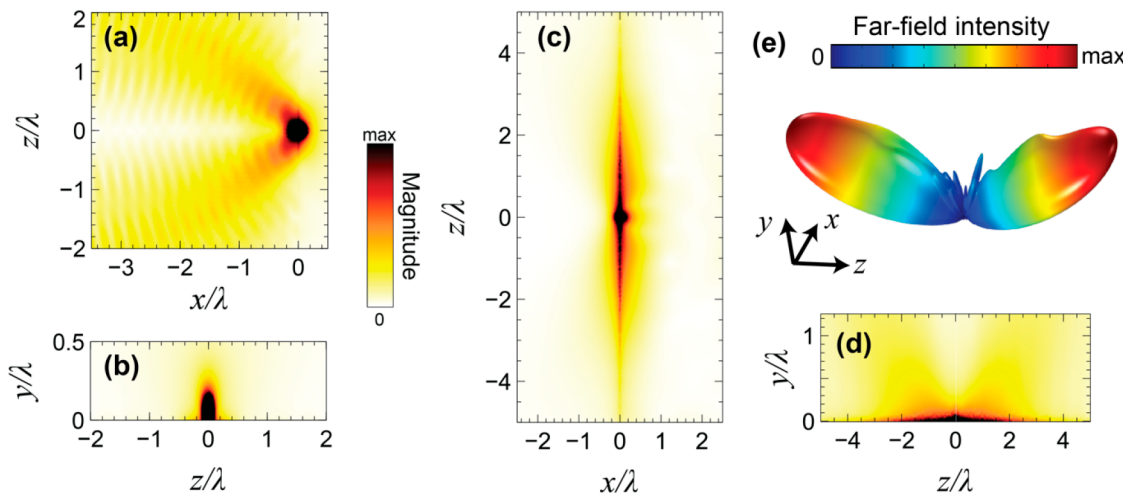


Figure 5. Effects of gain and leakage. (a, b) Numerically computed in-plane ($y = 0.01\lambda$) and out-of-plane ($x = 0$) electric-field magnitude maps in false-color scale, respectively, for an impedance junction with $\bar{Z}_1 = i0.5$ and $\bar{Z}_2 = 0.5 + i0.5$ (i.e., no gain). (c, d) Corresponding maps for a PT-symmetric impedance junction with $\bar{R} = 1.1$ and $\bar{X} = 0.1$ ($|\bar{Z}| > 1$), showing the leakage effect. (e) Corresponding radiation pattern. The field is excited by a y -directed elementary electric dipole placed at $x = y = 0$ and $y = 0.02\lambda$.

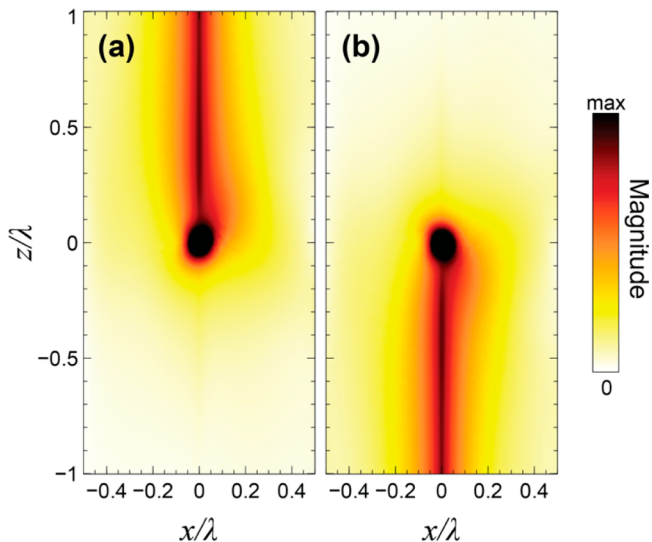


Figure 6. Chiral coupling. (a, b) Numerically computed in-plane ($y = 0.01\lambda$) electric-field magnitude maps in false-color scale, for a straight PT-symmetric impedance junction with $\bar{R} = 0.5$ and $\bar{X} = 0.5$, showing unidirectional propagation along the positive and negative z -direction, respectively. The field is excited by circularly polarized elementary sources of opposite handedness, synthesized via the superposition of an x -directed and a z -directed elementary electric dipole with the same amplitude and $\pm 90^\circ$ phase-lag, respectively, colocated at $x = z = 0$ and $y = 0.01\lambda$.

with δ parametrizing the gain/loss imbalance. As it may be expected (see Figure S5 of the Supporting Information), the effective index for this section is complex-valued, with negative imaginary part $\delta > 0$. Therefore, the imbalanced section effectively behaves as an amplifying cavity, connected with PT-symmetric input/output sections. Figure 7b shows the numerically computed transmission coefficient for this configuration, as a function of the cavity length L and the imbalance parameter δ . We observe the presence of a very large maximum ($\sim 10^3$), indicative of lasing. The corresponding in-plane and out-of-plane field maps shown in Figures 7c and d, respectively, confirm the localization properties typical of line

waves. The longitudinal cut shown in Figure 7e clearly shows the Fabry–Perot-type standing-wave pattern typical of lasing cavities. The above results set the stage for the development of novel types of flat-optics nanolasers, with emission strongly localized along a predefined 1-D path. Considering $\delta < 0$, the same working principle can be exploited to attain coherent perfect absorption.

Topological Aspects. Line waves in non-Hermitian structures have also been observed at the interface between PT-symmetric topological insulators,⁴⁴ which admit a photonic implementation in terms of graphene-based photonic crystals. We highlight that our proposed mechanism here differs substantially from these scenarios, as it does not rely on bandgaps. In fact, the basic constituents in our configuration are homogeneous, isotropic metasurfaces which, for an appropriate polarization different from the one of our line waves, would separately support attenuated or amplified surface waves. From the topological point of view, there are also fundamental differences with respect to conventional line waves in dual-reactance configurations.¹³ Similar to our case, the formation of a line wave at a reactive metasurface junction does not rely on a bandgap mechanism. From a physical viewpoint, it can be understood in terms of the complementary nature of the capacitive and inductive halves, which can support TM and TE surface waves, respectively. Mathematically, this can be expressed in terms of a duality condition that endows symmetry-protected pseudospin transport,⁴⁵ that is, topological-like robustness with respect to structural defects that do not violate pseudospin-degeneracy or imply the reversal of boundary conditions.¹³ Conversely, our proposed non-Hermitian line waves do not rely on the duality principle, but rather on the PT-symmetry condition in eq 3. Therefore, the above pseudospin arguments do not apply here and, different from conventional line waves, spin-filtered waveguiding is not generally attainable.⁴⁵ Nevertheless, as it can be observed from the standing-wave patterns in Figures 4c,d and S4 of the Supporting Information, defect-induced reflections remain localized along the trajectory, and both in-plane and out-of-plane scattering is markedly damped.

As an alternative physical explanation, while conventional line waves may be paralleled with the interface modes at an ϵ

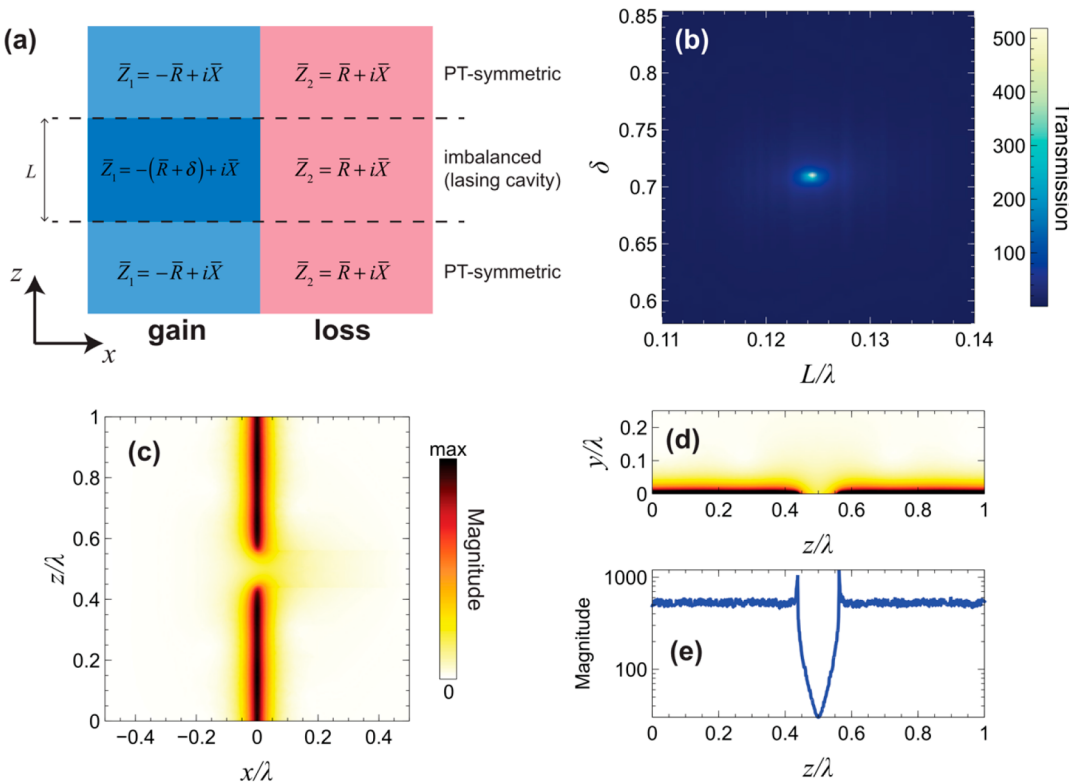


Figure 7. Lasing condition. (a) Schematic of a PT-symmetric impedance junction perturbed by an imbalanced section (see eq 8) acting as a lasing cavity. (b) Transmission-coefficient magnitude for $\bar{R} = 0.5$ and $\bar{X} = 0.1$, as a function of the cavity length L and the imbalance parameter δ , numerically computed by normalizing the electric field transmitted through the cavity by the incident one (computed in the absence of the cavity). (c, d) Numerically computed in-plane ($y = 0.01\lambda$) and out-of-plane ($x = 0$) electric-field magnitude maps in false-color scale, respectively, at the lasing condition $L = 0.124$, $\delta = 0.710$. (e) Corresponding longitudinal cut ($x = 0$, $y = 0.01\lambda$) of electric-field magnitude normalized with respect to the incident one. The field is excited by a y -directed elementary electric dipole placed at $x = 0$, $y = 0.01\lambda$, $z = 0.5\lambda$ (outside the domains visualized); the cavity is centered at $z = 0.5\lambda$.

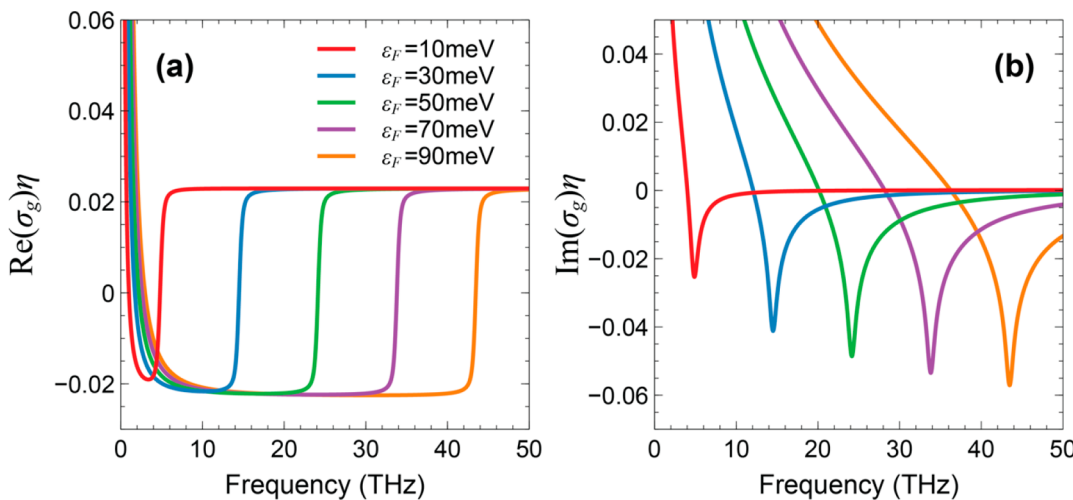


Figure 8. Possible graphene-based implementation. (a, b) Real and imaginary part, respectively, of the normalized optical conductivity of a photoexcited graphene monolayer, as a function of the frequency, for $T = 3$ K, $\tau = 1$ ps, and different values of the quasi-Fermi energy (see the Supporting Information for details).

negative/ μ -negative boundary,¹³ our non-Hermitian line waves should be compared with the interface modes at a boundary between complex-conjugated permittivities (or permeabilities, depending on the polarization).³³

Possible Implementations. Metasurfaces with capacitive and inductive character can be practically implemented in several configurations, depending on the operational frequency

of interest. Previous studies on conventional line waves have considered complementary patterned (patch/hole) metallic films laid on grounded dielectric substrates for microwave frequencies¹³ and metallic patches laid on a graphene layer for terahertz frequencies.¹⁵ Indeed, graphene-based implementations seem particularly attractive in view of the possibility of active manipulation and reconfigurability.

In the non-Hermitian scenario of interest here, for the lossy section, the inherent material losses can be exploited and possibly tailored via suitable doping. As for the gain section, negative-resistance elements based on amplifiers⁴⁶ or tunnel diodes⁴⁷ may be exploited at microwave frequencies, whereas possible terahertz implementations could rely on photoexcited graphene.^{25,26} Although this study is focused on the basic phenomenology, with a view toward possible practical implementations, it is important to assess to what extent typical models that are reported in the literature for photoexcited graphene are compatible with the gain requirements for supporting non-Hermitian line waves.

Referring to the *Supporting Information* for more details, we consider an optically pumped graphene monolayer which, in the terahertz regime, can exhibit population inversion and negative dynamic conductivity. For typical parameters reported in the topical literature,^{25,26} Figure 8 shows the optical conductivity as a function of frequency. As it may be observed, the real part can become negative within certain frequency ranges, depending on the value of the quasi-Fermi energy. In particular, there is a sharp transition between symmetric limiting values $\sim \pm 0.02\eta$ (see the *Supporting Information* for details), accompanied by an essentially inductive character. We recall that the surface impedance of a free-standing graphene sheet is related to the optical conductivity by¹⁵

$$Z_s = \frac{2}{\sigma_g} \quad (9)$$

with the factor 2 accounting for the two-faced character. As a consequence, the dispersion properties in Figure 8 indicate that a wide variety of inductive surface impedances with gain levels compatible with the appropriate bound-mode condition $|Z| > 1$ in eq 5 can be, in principle, synthesized by acting on the frequency and quasi-Fermi energy. Synthesizing the PT-symmetric lossy counterpart is less challenging from the technological viewpoint and it may be addressed in various ways via a suitably patterned metasurface. In fact, the dispersion characteristics in Figure 5 suggest that it is possible, in principle, to synthesize the lossy part from the same graphene sheet, by varying the quasi-Fermi energy. For instance, at a frequency of 46.3 THz, with quasi-Fermi energy levels of 115 and 10 meV, we obtain the normalized surface impedances $\bar{Z}_{s1} = -88.70 - i0.489$ and $\bar{Z}_{s2} = -87.18 - i0.490$, respectively, which approximately satisfy the required PT-symmetry condition. As detailed in the *Supporting Information*, the quasi-Fermi energy can be controlled via optical pumping and doping, so that one may envision a configuration featuring an optically pumped graphene sheet with different dopings in the two halves. The quasi-Fermi energy levels reported above are in line with values that were experimentally observed in the absence and presence of doping, under constant optical pumping.⁴⁸ Clearly, patterning the graphene or a superposed metallic sheet would endow additional degrees of freedom for tailoring the reactive response.^{15,25} In any case, it is worth remarking that, in view of the inherent restrictions imposed by causality, the PT-symmetry condition cannot be exactly obtained over extended spectral ranges, but only at isolated frequencies.^{25,49} Overall, it appears that a terahertz implementation based on photoexcited graphene is within reach for current or near-future technologies.

CONCLUSIONS

We have shown that PT-symmetric metasurface junctions can support line waves that can propagate unattenuated along the 1-D gain-loss interface while maintaining a tight localization both in-plane and out-of-plane. For these non-Hermitian line waves, we have related the waveguiding conditions to simple bounds in the complex impedance plane, and have investigated the propagation characteristics and underlying mechanisms analytically and numerically. In particular, we have explored and illustrated a number of interesting features, in terms of confinement, reconfigurability, lasing, and chiral coupling, also highlighting similarities and key differences with respect to conventional line waves. Finally, we have explored their technological feasibility, showing that the gain levels required are compatible with those attainable from realistic models available in the literature for photoexcited graphene at terahertz frequencies.

Overall, our study demonstrates a novel waveguiding mechanism for in-plane routing of signals in flat-optics scenarios based on non-Hermitian physics, which opens new pathways in a variety of applications, including reconfigurable photonics, lasers, and coherent perfect absorbers, microfluidics and micro-optomechanical systems, and quantum optics. Besides exploring these applications, our current and future research agenda is focused on studying more general non-Hermitian configurations beyond PT-symmetry (including fully passive and possibly anisotropic ones) and on a deeper evaluation of realistic technological platforms for the implementation.

METHODS

Analytic Modeling. For the calculation of the effective index in the eigenmode analysis, we rely on a generalized Sommerfeld–Maliuzhinets method²⁹ (see the *Supporting Information* for more details).

Numerical Simulations. Our numerical simulations rely on the finite-element-based commercial software package COMSOL Multiphysics.⁵⁰ Specifically, for the eigenmode analysis (Figures 2b and 3 and S1–S3 and S5 of the *Supporting Information*), we consider a 2-D computational domain comprising a semicircle of radius 2λ terminated by a perfectly matched layer (PML) of thickness 0.5λ , with the impedance boundary condition at $y = 0$ enforced via a surface current density ($J_x = E_x/Z$, $J_y = 0$, $J_z = E_z/Z$). The domain is discretized with an adaptive mesh with element size $\leq 0.01\lambda$ (and $\leq 0.001\lambda$ nearby the impedance surface), resulting in ~ 3 million degrees of freedom. We utilize the “Mode Analysis” study available in the RF Module, with the MUMPS direct solver and default parameters.

For the study of source-excited configurations (Figures 4–7 and Figure S4 of the *Supporting Information*), we consider a 3-D parallelepiped computational domain with a transverse size (along x) ranging from λ to 5λ (depending on the example), length (along z) of $\sim 8\lambda$, and height (along y) of $\sim \lambda$, terminated by a PML of thickness 0.25λ and the same impedance boundary condition at $y = 0$. In order to simulate an infinite impedance surface along the z -direction, at both ends we add fictitious sections of length 4λ , with linearly tapered resistance and a reactance profile that are eventually matched with the vacuum characteristic impedance at the PML. An adaptive meshing with element size $\leq 0.1\lambda$ (and $\leq 0.02\lambda$ nearby the impedance surface), resulting in ~ 5 million

degrees of freedom. Depending on the examples, the structure is excited by one or two elementary electric dipoles, with characteristics specified in the figure captions. The problem is solved via a frequency-domain analysis, with the Pardiso direct solver and default parameters. The radiation pattern in Figure 5e, is obtained by means of a near- to far-field transformation implemented in the far-field option available in the postprocessing tools.

ASSOCIATED CONTENT

Supporting Information

The Supporting Information is available free of charge at <https://pubs.acs.org/doi/10.1021/acsphtronics.0c00465>.

Details on analytic modeling and additional results ([PDF](#))

AUTHOR INFORMATION

Corresponding Author

Vincenzo Galdi — *Fields and Waves Lab, Department of Engineering, University of Sannio, I-82100 Benevento, Italy;*
✉ orcid.org/0000-0002-4796-3600; Email: vgaldi@unisannio.it

Authors

Massimo Moccia — *Fields and Waves Lab, Department of Engineering, University of Sannio, I-82100 Benevento, Italy*
Giuseppe Castaldi — *Fields and Waves Lab, Department of Engineering, University of Sannio, I-82100 Benevento, Italy*
Andrea Alù — *Photonics Initiative, Advanced Science Research Center and Physics Program, Graduate Center, City University of New York, New York, New York 10031, United States*

Complete contact information is available at:
<https://pubs.acs.org/10.1021/acsphtronics.0c00465>

Author Contributions

G.C., A.A., and V.G. conceived the idea. M.M. and G.C. carried out the modeling and numerical simulations. A.A. and V.G. supervised the study. All authors contributed to the data analysis and interpretation. V.G. wrote the manuscript with inputs and feedback from all authors.

Funding

This work was supported in part by the University of Sannio (FRA program) and the Air Force Office of Scientific Research.

Notes

The authors declare no competing financial interest.

REFERENCES

- (1) Holloway, C. L.; Dienstfrey, A.; Kuester, E. F.; O'Hara, J. F.; Azad, A. K.; Taylor, A. J. A Discussion on the Interpretation and Characterization of Metafilms/Metasurfaces: The Two-Dimensional Equivalent of Metamaterials. *Metamaterials* **2009**, *3*, 100–112.
- (2) Yu, N.; Genevet, P.; Kats, M. A.; Aieta, F.; Tétienne, J.-P.; Capasso, F.; Gaburro, Z. Light Propagation with Phase Discontinuities: Generalized Laws of Reflection and Refraction. *Science* **2011**, *334*, 333–337.
- (3) Nanfang, Y.; Genevet, P.; Aieta, F.; Kats, M. A.; Blanchard, R.; Aoust, G.; Tétienne, J.-P.; Gaburro, Z.; Capasso, F. Flat Optics: Controlling Wavefronts With Optical Antenna Metasurfaces. *IEEE J. Sel. Top. Quantum Electron.* **2013**, *19*, 4700423.
- (4) Yu, N.; Capasso, F. Flat Optics with Designer Metasurfaces. *Nat. Mater.* **2014**, *13*, 139–150.
- (5) Bao, Q.; Hoh, H. Y. *2D Materials for Photonic and Optoelectronic Applications*; Woodhead Publishing: Sawston, U.K., 2019.
- (6) Gomez-Diaz, J. S.; Alù, A. Flatland Optics with Hyperbolic Metasurfaces. *ACS Photonics* **2016**, *3*, 2211–2224.
- (7) Vakil, A.; Engheta, N. Transformation Optics Using Graphene. *Science* **2011**, *332*, 1291–1294.
- (8) Yang, R.; Hao, Y. An Accurate Control of the Surface Wave Using Transformation Optics. *Opt. Express* **2012**, *20*, 9341–9350.
- (9) Patel, A. M.; Grbic, A. Transformation Electromagnetics Devices Based on Printed-Circuit Tensor Impedance Surfaces. *IEEE Trans. Microwave Theory Tech.* **2014**, *62*, 1102–1111.
- (10) Mencagli, M., jr; Martini, E.; González-Ovejero, D.; Maci, S. Metasurfing by Transformation Electromagnetics. *IEEE Antennas Wireless Propagat. Lett.* **2014**, *13*, 1767–1770.
- (11) Mencagli, M., jr; Martini, E.; González-Ovejero, D.; Maci, S. Metasurface Transformation Optics. *J. Opt.* **2014**, *16*, 125106.
- (12) Horsley, S. A. R.; Hooper, I. R. One Dimensional Electromagnetic Waves on Flat Surfaces. *J. Phys. D: Appl. Phys.* **2014**, *47*, 435103.
- (13) Bisharat, D. J.; Sievenpiper, D. F. Guiding Waves Along an Infinitesimal Line between Impedance Surfaces. *Phys. Rev. Lett.* **2017**, *119*, 106802.
- (14) Ozawa, T.; Price, H. M.; Amo, A.; Goldman, N.; Hafezi, M.; Lu, L.; Rechtsman, M. C.; Schuster, D.; Simon, J.; Zilberberg, O.; Carusotto, I. Topological Photonics. *Rev. Mod. Phys.* **2019**, *91*, 015006.
- (15) Bisharat, D. J.; Sievenpiper, D. F. Manipulating Line Waves in Flat Graphene for Agile Terahertz Applications. *Nanophotonics* **2018**, *7*, 893–903.
- (16) Bisharat, D. J.; Sievenpiper, D. F. Electromagnetic-Dual Metasurfaces for Topological States along a 1D Interface. *Laser Photonics Rev.* **2019**, *13*, 1900126.
- (17) Bender, C. M.; Boettcher, S. Real Spectra in Non-Hermitian Hamiltonians Having PT Symmetry. *Phys. Rev. Lett.* **1998**, *80*, 5243–5246.
- (18) El-Ganainy, R.; Makris, K. G.; Khajavikhan, M.; Musslimani, Z. H.; Rotter, S.; Christodoulides, D. N. Non-Hermitian Physics and PT Symmetry. *Nat. Phys.* **2018**, *14*, 11–19.
- (19) Feng, L.; El-Ganainy, R.; Ge, L. Non-Hermitian Photonics Based on Parity-Time Symmetry. *Nat. Photonics* **2017**, *11*, 752–762.
- (20) El-Ganainy, R.; Khajavikhan, M.; Christodoulides, D. N.; Ozdemir, S. K. The Dawn of Non-Hermitian Optics. *Commun. Phys.* **2019**, *2*, 37.
- (21) Fleury, R.; Sounas, D. L.; Alù, A. Negative Refraction and Planar Focusing Based on Parity-Time Symmetric Metasurfaces. *Phys. Rev. Lett.* **2014**, *113*, 023903.
- (22) Sounas, D. L.; Fleury, R.; Alù, A. Unidirectional Cloaking Based on Metasurfaces with Balanced Loss and Gain. *Phys. Rev. Appl.* **2015**, *4*, 014005.
- (23) Monticone, F.; Valagiannopoulos, C. A.; Alù, A. Parity-Time Symmetric Nonlocal Metasurfaces: All-Angle Negative Refraction and Volumetric Imaging. *Phys. Rev. X* **2016**, *6*, 041018.
- (24) Savoia, S.; Valagiannopoulos, C. A.; Monticone, F.; Castaldi, G.; Galdi, V.; Alù, A. Magnified Imaging Based on Non-Hermitian Nonlocal Cylindrical Metasurfaces. *Phys. Rev. B: Condens. Matter Mater. Phys.* **2017**, *95*, 115114.
- (25) Chen, P.-Y.; Jung, J. PT Symmetry and Singularity-Enhanced Sensing Based on Photoexcited Graphene Metasurfaces. *Phys. Rev. Appl.* **2016**, *5*, 064018.
- (26) Sakhdari, M.; Farhat, M.; Chen, P.-Y. PT-Symmetric Metasurfaces: Wave Manipulation and Sensing Using Singular Points. *New J. Phys.* **2017**, *19*, 065002.
- (27) Sakhdari, M.; Estakhri, N. M.; Bagci, H.; Chen, P.-Y. Low-Threshold Lasing and Coherent Perfect Absorption in Generalized PT-Symmetric Optical Structures. *Phys. Rev. Appl.* **2018**, *10*, 024030.
- (28) Zhang, X.; Zhang, Z.; Wang, Q.; Zhu, S.; Liu, H. Controlling Thermal Emission by Parity-Symmetric Fano Resonance of Optical Absorbers in Metasurfaces. *ACS Photonics* **2019**, *6*, 2671–2676.

- (29) Kong, X.; Bisharat, D. J.; Xiao, G.; Sievenpiper, D. F. Analytic Theory of an Edge Mode between Impedance Surfaces. *Phys. Rev. A: At., Mol., Opt. Phys.* **2019**, *99*, 033842.
- (30) Senior, T. B.; Volakis, J. L. *Approximate Boundary Conditions in Electromagnetics*; Institution of Electrical Engineers: London, U.K., 1995.
- (31) Hoppe, D. J.; Rahmat-Samii, Y. *Impedance Boundary Conditions in Electromagnetics*; Electromagnetics library series; Taylor & Francis: Washington, DC, 1995.
- (32) Savoia, S.; Castaldi, G.; Galdi, V.; Alù, A.; Engheta, N. Tunneling of Obliquely Incident Waves through PT-Symmetric Epsilon-near-Zero Bilayers. *Phys. Rev. B: Condens. Matter Mater. Phys.* **2014**, *89*, 085105.
- (33) Savoia, S.; Castaldi, G.; Galdi, V.; Alù, A.; Engheta, N. PT-Symmetry-Induced Wave Confinement and Guiding in ϵ -near-Zero Metamaterials. *Phys. Rev. B: Condens. Matter Mater. Phys.* **2015**, *91*, 115114.
- (34) Savoia, S.; Castaldi, G.; Galdi, V. Non-Hermiticity-Induced Wave Confinement and Guiding in Loss-Gain-Loss Three-Layer Systems. *Phys. Rev. A: At., Mol., Opt. Phys.* **2016**, *94*, 043838.
- (35) Maluzhinets, G. D. Excitation, Reflection and Emission of Surface Waves from a Wedge with Given Face Impedances. *Sov. Phys.-Dokl.* **1958**, *3*, 752–755.
- (36) Vaccaro, V. G. The Generalized Reflection Method in Electromagnetism. *Arch. Elektron. Uebertraeg.* **1980**, *34*, 493–500.
- (37) Snyder, A. W.; Love, J. D. *Optical Waveguide Theory*; Springer US: Boston, MA, 1983.
- (38) Meixner, J. The Behavior of Electromagnetic Fields at Edges. *IRE Trans. Antennas Propag.* **1972**, *20*, 442–446.
- (39) Miri, M.-A.; Cotrufo, M.; Alù, A. Anomalous Optical Forces in PT-Symmetric Waveguides. *Opt. Lett.* **2019**, *44*, 3558–3561.
- (40) Harrington, R. F. *Time-Harmonic Electromagnetic Fields*; Wiley-IEEE Press: Piscataway, NJ, 2001.
- (41) Jackson, D. R.; Oliner, A. A. Leaky-Wave Antennas. In *Modern Antenna Handbook*; Balanis, C. A., Ed; John Wiley & Sons: New York, NY, 2007; pp 325–367.
- (42) Van Mechelen, T.; Jacob, Z. Universal Spin-Momentum Locking of Evanescent Waves. *Optica* **2016**, *3*, 118–126.
- (43) Lodahl, P.; Mahmoodian, S.; Stobbe, S.; Rauschenbeutel, A.; Schneeweiss, P.; Volz, J.; Pichler, H.; Zoller, P. Chiral Quantum Optics. *Nature* **2017**, *541*, 473–480.
- (44) Ni, X.; Smirnova, D.; Poddubny, A.; Leykam, D.; Chong, Y.; Khanikaev, A. B. PT Phase Transitions of Edge States at PT Symmetric Interfaces in Non-Hermitian Topological Insulators. *Phys. Rev. B: Condens. Matter Mater. Phys.* **2018**, *98*, 165129.
- (45) Chen, W.-J.; Zhang, Z.-Q.; Dong, J.-W.; Chan, C. T. Symmetry-Protected Transport in a Pseudospin-Polarized Waveguide. *Nat. Commun.* **2015**, *6*, 8183.
- (46) Chen, L.; Ma, Q.; Jing, H. B.; Cui, H. Y.; Liu, Y.; Cui, T. J. Space-Energy Digital-Coding Metasurface Based on an Active Amplifier. *Phys. Rev. Appl.* **2019**, *11*, 054051.
- (47) Ye, D.; Chang, K.; Ran, L.; Xin, H. Microwave Gain Medium with Negative Refractive Index. *Nat. Commun.* **2014**, *5*, 5841.
- (48) Kar, S.; Mohapatra, D. R.; Freysz, E.; Sood, A. K. Tuning Photoinduced Terahertz Conductivity in Monolayer Graphene: Optical-Pump Terahertz-Probe Spectroscopy. *Phys. Rev. B: Condens. Matter Mater. Phys.* **2014**, *90*, 165420.
- (49) Zyablovsky, A. A.; Vinogradov, A. P.; Dorofeenko, A. V.; Pukhov, A. A.; Lisansky, A. A. Causality and Phase Transitions in PT-Symmetric Optical Systems. *Phys. Rev. A: At., Mol., Opt. Phys.* **2014**, *89*, 033808.
- (50) COMSOL Multiphysics v. 5.1; COMSOL AB, Stockholm, Sweden.